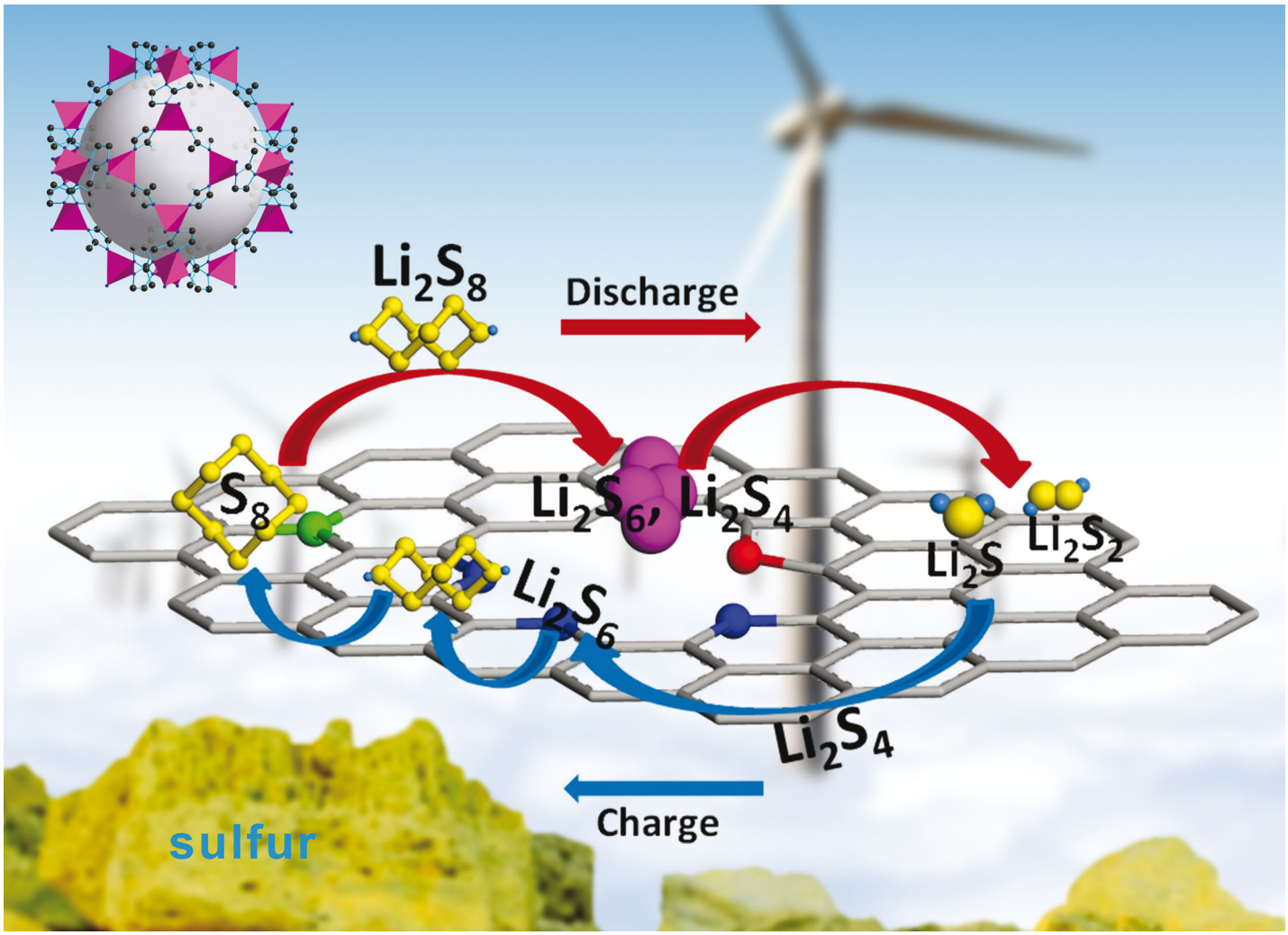

Showcasing research from Prof. Quanfeng Dong's group at Xiamen University, China

A novel synergistic composite with multi-functional effects for high-performance Li–S batteries

Lithium–sulfur (Li–S) batteries are becoming one of the most attractive electrochemical energy storage systems. We developed a multi-functionalized composite in which the entrapping for polysulfide, the catalyzing for S redox and an ideal electronic conductive network were synchronously achieved, and hence improved the Li–S performance significantly. Aiming at the main issues of Li–S batteries, such an approach has provided a comprehensive solution strategy.

As featured in:

See Ming-Sen Zheng, Quan-Feng Dong *et al.*, *Energy Environ. Sci.*, 2016, **9**, 1998.

ROYAL SOCIETY OF CHEMISTRY

www.rsc.org/ees

Registered charity number: 207890

Energy & Environmental Science

COMMUNICATION

View Article Online
View Journal | View Issue

Cite this: *Energy Environ. Sci.*, 2016, **9**, 1998

Received 12th January 2016,
Accepted 10th March 2016

DOI: 10.1039/c6ee00104a

www.rsc.org/ees

A novel synergistic composite with multi-functional effects for high-performance Li–S batteries†

Yi-Juan Li,‡ Jing-Min Fan,‡ Ming-Sen Zheng* and Quan-Feng Dong*

The rechargeable lithium–sulfur battery is regarded as a promising option for electrochemical energy storage systems owing to its high energy density, low cost and environmental friendliness. Further development of the Li–S battery, however, is still impeded by capacity decay and kinetic sluggishness caused by the polysulfide shuttle and electrode/electrolyte interface issues. Herein, a new type of metal–organic-framework-derived sulfur host containing cobalt and N-doped graphitic carbon (Co–N-GC) was synthesized and reported, in which the catalyzing for S redox,entrapping of polysulfides and an ideal electronic matrix were successfully achieved synchronously, leading to a significant improvement in the Li–S performance. The large surface area and uniform dispersion of cobalt nanoparticles within the N-doped graphitic carbon matrix contributed to a distinct enhancement in the specific capacity, rate performance and cycle stability for Li–S batteries. As a result of this multi-functional arrangement, cathodes with a high sulfur loading of 70 wt% could operate at 1C for over 500 cycles with nearly 100% coulombic efficiency and exhibited an outstanding high-rate response of up to 5C, suggesting that the S@Co–N-GC electrode was markedly improved by the proposed strategy, demonstrating its great potential for use in low-cost and high-energy Li–S batteries.

Broader context

The demand for energy grows with each passing day due to population and economic growth and advances in lifestyles. Lithium–sulfur (Li–S) batteries are becoming attractive due to their extremely high theoretical energy density (2600 W h^{-1} kg^{-1}) and low toxicity. However, severe capacity decay and kinetic sluggishness associated with polysulfide shuttling and electrode/electrolyte interface issues still remain a big challenge, hindering the practical applications of this technology. Herein, we developed a multi-functionalized composite derived from metal–organic-frameworks (MOFs) containing a cobalt and N-doped graphitic carbon (Co–N-GC) matrix, in which the entrapping of polysulfides, the catalyzing for S redox and an ideal electronic conductive network were successfully achieved synchronously, leading to a significant improvement in the Li–S performance. With an aim to overcome the aforementioned problems, such an approach provides a comprehensive solution strategy.

As the most promising rechargeable battery system, lithium–sulfur (Li–S) batteries can deliver a high theoretical specific capacity of 1675 mA h^{-1} g^{-1} based on the complete conversion reaction of sulfur with lithium metal to form lithium sulfide (Li_2S).[1,2] In addition, the cathode material, sulfur, is one of the most abundant elements in the earth's crust and also has the advantage of low cost.[3] The potential use of sulfur as a cathode material has long been studied, however, several severe obstacles have hindered the realization of Li–S batteries. On the one hand, sulfur exhibits poor electrochemical activity because of its insulating nature, which has led to the low utilization of sulfur. In addition, lithium polysulfides formed during the charge/discharge electrochemical process are easily dissolved in organic electrolytes[4] and are able to "shuttle" between the electrodes, resulting in a rapid fading of capacity and high self-discharge.[5]

Over the past few decades, considerable strategies have been developed to address these issues. Among these attempts, the use of sulfur-containing composites has been demonstrated to be an effective way to overcome the low conductivity of sulfur. Conductive polymers[6–8] and porous carbons[9–12] have been reported as common candidates to form composites with sulfur. Moreover, porous carbon could provide an exceptionally high surface area to disperse sulfur, which could also diminish the negative effect of the polysulfides shuttling between the electrodes by retaining polysulfides at the cathode region through the absorbability of the high surface-area carbon.[13] Recently, metal–organic frameworks (MOFs) consisting of metal ions (clusters) have been studied as novel sulfur hosts in Li–S batteries.[14–16] In particular, MOFs are very attractive as both a template and precursor for the fabrication of nanostructure materials such as porous carbons and metal oxides.[17,18] Compared with many other highly porous carbon materials, the porous carbon derived from MOFs exhibits

Department of Chemistry, College of Chemistry and Chemical Engineering, Xiamen University Collaborative Innovation Centre of Chemistry for Energy Materials, State Key Lab. of Physical Chemistry of Solid Surfaces, Xiamen, Fujian, 361005, China. E-mail: qfdong@xmu.edu.cn, mszheng@xmu.edu.cn; Fax: (+86)0592-2183905; Tel: (+86)0592-2185905

† Electronic supplementary information (ESI) available. See DOI: 10.1039/c6ee00104a

‡ These authors have contributed equally.

a highly uniform porosity owing to the ordered crystalline structures of MOFs.[19,20] These MOF-derived materials are promising candidates in gas storage,[21,22] electrochemical capacitors, electrocatalysis[20,23,24] and lithium ion batteries.[18,25] In addition to encapsulate sulfur within the pores of carbon materials or conductive polymer matrixes, high-surface-area polar metallic oxides have been recently used to provide both a "sulfiphilic" surface and to supply electron transport to effect surface-enhanced redox chemistry,[26] or to spatially locate Li_2S deposition and enhance redox.[27] Nazar *et al.* presented manganese dioxide as a highly efficient polysulfide mediator that relies on mediating polysulfide redox through an insoluble thiosulfate species in a two-step process.[28] Moreover, Jie Xiao *et al.* demonstrated strong Lewis acid–base interactions between Ni-MOF and polysulfides in Li–S batteries.[29] More recently, Babu G *et al.*[30,31] proposed that the polysulfide shuttle process in the Li–S cell could be controlled by electrocatalysis. They found that Pt/graphene and Ni/graphene exhibited a reduced overpotential and excellent specific capacity over pristine graphene electrodes. Actually, introducing a catalyst in the Li–S system to modify the electrode/electrolyte interface presents a new method for improving electrochemical performance. It is very crucial to design an electrode in which not only the electrochemical processes of S could be improved but also an ideal matrix that could effectively entrap the intermediate polysulfide.

Herein, we successfully developed a facile synthesis approach to obtain a novel 3D porous N-doped graphitic carbon–Co composite (Co–N-GC) by using MOF polyhedron (ZIF-67) as the precursor. The composite was employed as a carbon host to embed sulfur for Li–S batteries. As a subclass of MOFs, ZIF-67 consists of cobalt ions as the metal centres and 2-methylimidazole as the N-containing ligands.[24] Benefiting from both the special crystalline structure and abundant uniform micropores, the as-prepared Co–N-GC composite host not only facilitates electron and ion transfer during the discharge–charge reactions, but also efficiently prevents polysulfide dissolution. Furthermore, Co nanoparticles are uniformly dispersed in the N-doped carbon matrix by taking advantage of the confinement effect of porous carbon structure, and the catalytic effect arising from such high Co distribution also plays a key role during the discharge and charge process cycles of Li–S batteries. These unique properties are expected to significantly enhance the resulting Li–S performance. With a high sulfur content of 70 wt% in the composite, the S@Co–N-GC delivered a specific capacity of 1670 mA h^{-1} g^{-1} at 0.05C according to S content, which is almost the same as its theoretical specific capacity of 1675 mA h^{-1} g^{-1}. Moreover, it maintained a stable cycling performance at 1C over 500 cycles with nearly 100% coulombic efficiency.

The as-prepared ZIF-67 and the Co–N-GC composite were characterized by scanning electron microscopy (SEM) and transmission electron microscopy (TEM) (Fig. 1a–d). As shown in Fig. 1a, the as-prepared ZIF-67 had a uniform particle size of approximate 350 nm with a rhombic dodecahedral shape. Upon carbonization at the target temperature under N_2 atmosphere, the resulting Co–N-GC composite inherited the overall polyhedron-like morphology of the parent ZIF-67 and a similar size (Fig. 1b and c). The as-prepared ZIF-67 showed high crystallinity without

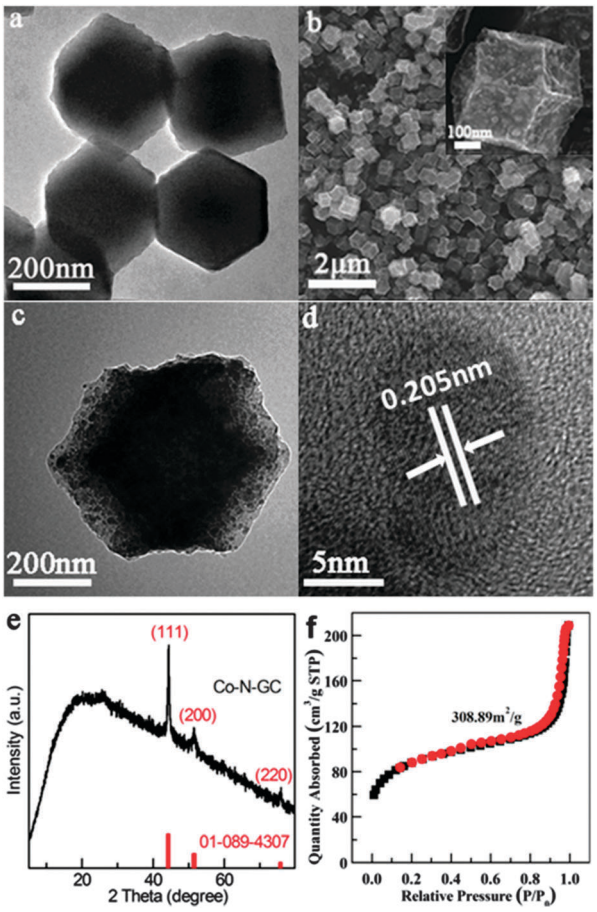

Fig. 1 (a) TEM image showing the morphology of the as-prepared ZIF-67. (b) Low- and high- (inset) magnification SEM images of the Co–N-GC composite. (c) Corresponding TEM image of the Co–N-GC composite. (d) High-resolution TEM image (HRTEM). (e) XRD pattern of the Co–N-GC composite. (f) N_2 adsorption–desorption analysis of the Co–N-GC composite.

any detectable by-products as revealed by the powder X-ray diffraction (XRD) pattern (Fig. S1a, ESI†). After annealing, the characteristic peaks of ZIF-67 disappeared completely, as shown in Fig. 1e. There were three apparent diffraction peaks at 2θ = 44.2°, 51.6° and 75.9°, which were in good agreement with the crystalline data of the cobalt nanoparticles. These peaks corresponded to the cobalt crystalline lattice facets of (111), (200) and (220), respectively, indicating that the cobalt ions in the frameworks were reduced to form cobalt nanoparticles. In addition, a small and broad peak at around 2θ = 26° suggested an improved graphitic crystallinity owing to the catalytic effect of cobalt during carbonization. The average Co particle sizes were estimated using the Scherrer equation, $d = 0.89\lambda/B\cos\theta$, where d is the average size of the Co particles, λ is the X-ray wavelength (Cu Kα, λ = 0.154 nm), B is the half-peak width for the Co(111) peak in radians and θ is the diffraction angle of the Co(111) reflection. The cobalt particles with a calculated size of 22.09 nm were homogenously distributed and embedded within the carbon matrix. An interspacing of 0.205 nm (Fig. 1d) accounted for the (111) lattice fringes of the cobalt particles, which was well consistent with the value (2.046 Å) calculated from the XRD data.

N_2 adsorption–desorption analysis was performed to further investigate the porous structure of the Co–N-GC composite. The Brunauer–Emmett–Teller (BET) surface area of Co–N-GC was measured to be 308.89 $m^2\ g^{-1}$ (Fig. 1f), and the typical type I Langmuir isotherm indicated the microporous structure (Fig. S1b, ESI†). The large surface area and abundant micropores were apt to entrapping the intermediate polysulfides.

The conversion of ZIF-67 to Co–N-GC *via* pyrolysis and its interaction with the lithium polysulfides during charge/discharge processes is illustrated schematically in Fig. 2. For the synthesis of the Co–N-GC composite, as-prepared ZIF-67 crystals were directly subjected to a thermal carbonization process in a N_2 atmosphere. The S@Co–N-GC composite was prepared *via* a melt-diffusion approach (see Experimental section in the ESI† for more details). To evaluate the S content in the S@Co–N-GC nanocomposite, thermogravimetric analysis (TGA) was carried out under a N_2 atmosphere at a heating rate of 10 °C min^{-1}. As shown in Fig. S2a (ESI†), the main weight loss between 150 and 300 °C was ascribed to the sublimation of incorporated sulfur in the N_2 atmosphere, indicating that the S@Co–N-GC nanocomposite had a sulfur content of about 70%. Moreover, from the XRD pattern of the Co–N-GC composite shown in Fig. S2b (ESI†), it can be seen that all the diffraction peaks are well indexed by the sulfur structure, indicating that sulfur was successfully incorporated in the Co–N-GC composite. As the SEM and TEM images in Fig. 3a–c revealed, the S@Co–N-GC composite resembles the pristine Co–N-GC composite. To further confirm the distribution of elemental S in the composite, the HAADF-STEM image and the corresponding element mapping of C, N, Co and S are displayed in Fig. 3d–h. The elemental distribution maps on a single S@Co–N-GC particle not only clearly reveal the homogenous distribution of S on the Co–N-GC surface, but also confirm the uniform presence of Co nanoparticles and the effective incorporation of N atoms into the carbon matrix.

Apart from the surface area and pore distribution, the Li–S battery performance was also improved by the synergic catalytic effect of cobalt and the nitrogen-containing groups present in the carbon matrix. In order to investigate the chemical composition in the Co–N-GC composite, X-ray photoelectron spectroscopy (XPS) was utilized. The fitted C 1s spectrum (Fig. 4a) showed a main peak at around 284.8 eV, corresponding to sp^2 carbon, and peaks at 285.8 eV and 287.6 eV, assigned to C═N bonds and C–N species, respectively. All the abovementioned results exactly confirmed the formation of C–N bonds during the annealing process. It was proved by our previous work that a N-doped carbon surface can serve as a conductive Lewis base "catalyst" matrix to enhance the adsorption energy of Li_2S_n (n = 4–8), which facilitates the oxidization of $Li_2S_6 \rightarrow Li_2S_8 \rightarrow S_8$ and thus improves the S utilization and cycle stability.[32] The presence of nitrogen species in the Co–N-GC composite was proved and investigated by analyzing the high-resolution N 1s XPS spectrum (Fig. 4b). In particular, the N 1s spectrum could be fitted into three characteristic peaks at binding energy of 398.9 eV, 400.4 eV and 401.3 eV, which corresponded to pyridinic, pyrrolic and graphitic nitrogen, respectively.[33] Obviously, the main N configuration in the Co–N-GC composite annealed at 700 °C is pyridinic-N, which is p-type doping and involves two p-electrons on the N atom. This implies that it should exhibit an excellent electrochemical performance as a conductive Lewis base matrix for the sulfur cathode. Moreover, the predominance

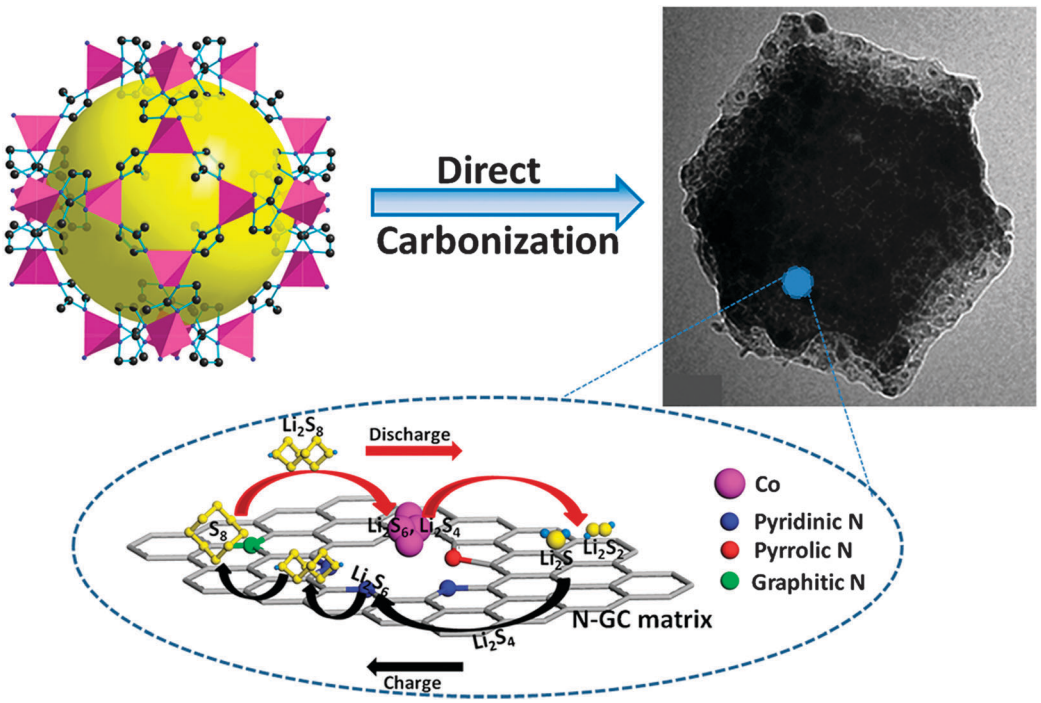

Fig. 2 Schematic illustration of a dual-catalyst anchored Co–N-GC composite preparation and its interaction with polysulfides during the charge/discharge processes of a Li–S battery.

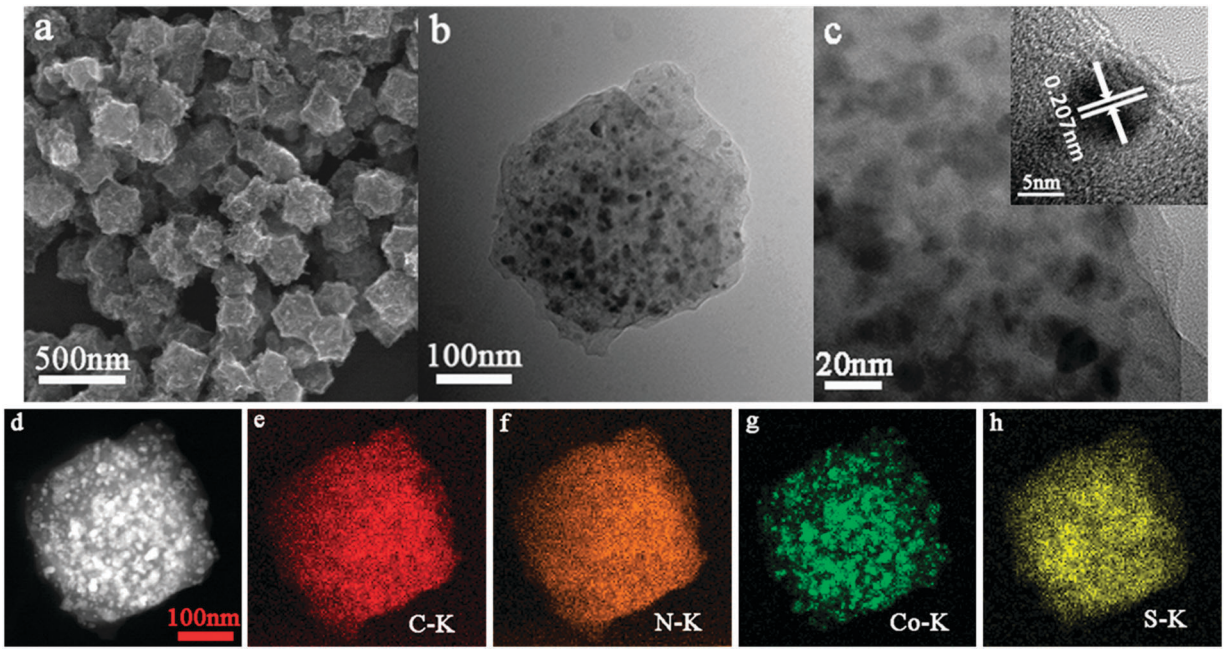

Fig. 3 (a) SEM image of the S@ Co–N-GC composite. (b) Low- and (c) high-magnification TEM images of the Co–N-GC composite (inset: the corresponding high-resolution TEM image (HRTEM) showing the lattice pattern of the Co particle). (d) The HAADF-STEM image of the S@ Co–N-GC composite and the corresponding elemental mapping of C (e), N (f), Co (g) and S (h).

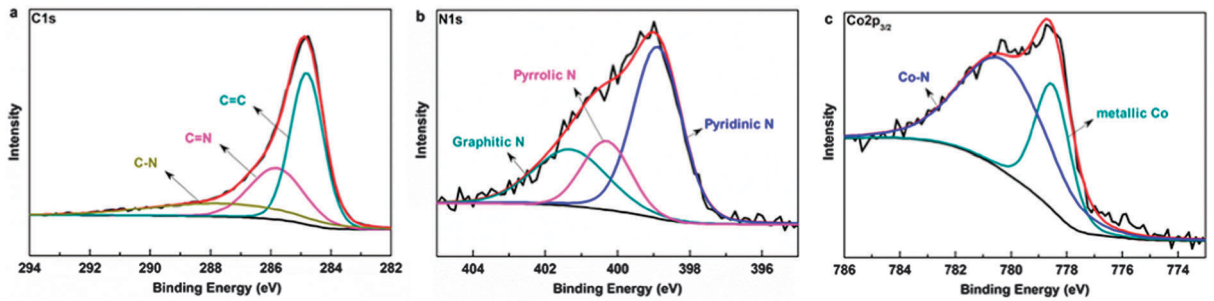

Fig. 4 (a) C 1s, (b) N 1s and (c) Co $2p_{3/2}$ X-ray photoelectron spectroscopy (XPS) of the as-prepared Co–N-GC composite. The spectra are shown with raw data and fitting data derived by Lorentz–Gaussian function.

of pyridinic and pyrrolic nitrogen could to some extent indirectly suggest the presence of Co–N_x.[34] The high-resolution Co $2p_{3/2}$ spectrum illustrated in Fig. 4c was deconvoluted into two characteristic peaks centred around 778.5 eV and 780.3 eV. The binding energy of metallic cobalt was detected at 778.5 eV, affirming the existence of metallic cobalt, while the peak at 780.3 eV could be attributed to divalent cobalt, which probably implies the incorporation of cobalt into the network consisting of a carbon matrix and the nitrogen species Co–N_x.[35] Pt and Ni have been proven to be promising electrocatalysts to convert short- to long-chain polysulfides efficiently during charging.[31] In addition, it has been confirmed that strong interactions exist between Lewis acidic Ni/Co(II) and polysulfide base.[29] Similarly, the presence of a Co catalyst may not only help to convert polysulfide (PS) deposits back to soluble long-chain polysulfides but can also catalyze long-chain polysulfides to Li_2S_2 and even to Li_2S and thus enhance the reaction kinetics and result in a high specific capacity. Based on the abovementioned results, a possible mechanism can be proposed to explain the enhanced performance of the MOF-derived Co–N-GC composite for a Li–S cell. First, the open 3D structure and high surface area (especially the micropores) facilitate ion transfer and polysulfide physical adsorption. Moreover, the synergistic Co–N plays an important role in the enhancement of Li–S performance. On the one hand, the presence of Co helps to increase the specific capacity and rate capability by effectively transforming long-chain polysulfides to short-chain ones; while on the other hand, doped-nitrogen is apt to improve the cycle performance by facilitating the oxidation of $Li_2S_6 \rightarrow Li_2S_8 \rightarrow S_8$, thus improving the S utilization. Therefore, in terms of catalyzing, the MOF-derived Co–N-GC composite thus plays a dual-catalyzing role during S reduction and oxidation in Li–S batteries.

Next, the Li/S@Co–N-GC cell was evaluated by galvanostatic discharge/charge at various current rates. As shown in Fig. 5a, the Li/S@Co–N-GC cell exhibited excellent rate performance. At the rate of 0.05C, it could deliver an extremely high specific

discharge capacity of 1670 mA h^{-1} g^{-1}, which is nearly the theoretical capacity of S, and a reversible charge capacity of 1651 mA h^{-1} g^{-1}, with a coulombic efficiency of 98.9% (the 1C-rate is defined as the current density of 1675 mA g^{-1}). The capacity faded in the subsequent cycles but stabilized at 1520 mA h^{-1} g^{-1} after five cycles. The capacity fading in the second cycle was ascribed to the unavoidable dissolution of polysulfide into the electrolyte. When the rate was increased to 0.1C, a specific capacity of 1350 mA h^{-1} g^{-1} was retained, which then slowly reduced to 1145 mA h^{-1} g^{-1} at 0.2C, 925 mA h^{-1} g^{-1} at 0.5C, 795 mA h^{-1} g^{-1} at 1C, 685 mA h^{-1} g^{-1} at 2C and 565 mA h^{-1} g^{-1} at 5C, before it finally recovered to 870 mA h^{-1} g^{-1} at 0.5C after 10 cycles. Furthermore, both the discharge and charge capacities were stable at different current densities and the coulombic efficiency was almost 100%, suggesting a perfect control of the so-called shuttle effect, which is regarded as the biggest disadvantage of a Li–S battery. Fig. 5b shows the corresponding discharge/charge voltage profiles of the S@Co–N-GC electrode at different current rates (0.05, 0.1, 0.2, 0.5, 1, 2 and 5C) in the potential range of 1.7–2.7 V. At low current rates, the discharge voltage profiles were characterized by a two-plateau (2.35 V and 2.05 V) behaviour of a typical S cathode, while the charge voltage profiles exhibited two platforms at around 2.39 V and 2.42 V, respectively. This was in good agreement with the reduction and oxidation peaks in the CV curves (Fig. S3, ESI†). According to the reported mechanisms for the reduction and oxidation of S during the discharge/charge process,[36] the first peak at 2.35 V corresponds to the reduction of S_8 to soluble high-order Li_2S_n ($4 \leq n \leq 8$), while the second peak at 2.05 V corresponds to the further reduction of the high-order Li_2S_n to Li_2S_2 and eventually, to Li_2S. The oxidation process of the cathode also occurs in two stages: the first oxidation peak at 2.39 V is associated with the formation of Li_2S_n, which is oxidized to S_8 at 2.42 V; while the second oxidation peak at around 2.42 V, it should be pointed out, is more distinct than that of the previously reported results, indicating the more complete oxidation of high-order Li_2S_n to S_8 on the Co–N-GC composite surface, which was attributed to the effective adsorption of Li_2S_n on the N-GC surface and the effective transformation of Li_2S_n to S_8 upon the Co–N dual-catalyst. Both the discharge and charge curves overlap well below the current rate of 1C, suggesting small polarization and a good rate capability, especially during the liquid-phase reaction processes. It can be noted that at larger current rates above 1C, both the discharge plateau and the discharge capacity decrease, which can be ascribed to the higher ohmic and kinetic overpotentials at higher current rates. However, apparent platforms can still be observed. The high S utilization and excellent rate performance of the S@Co–N-GC are likely to

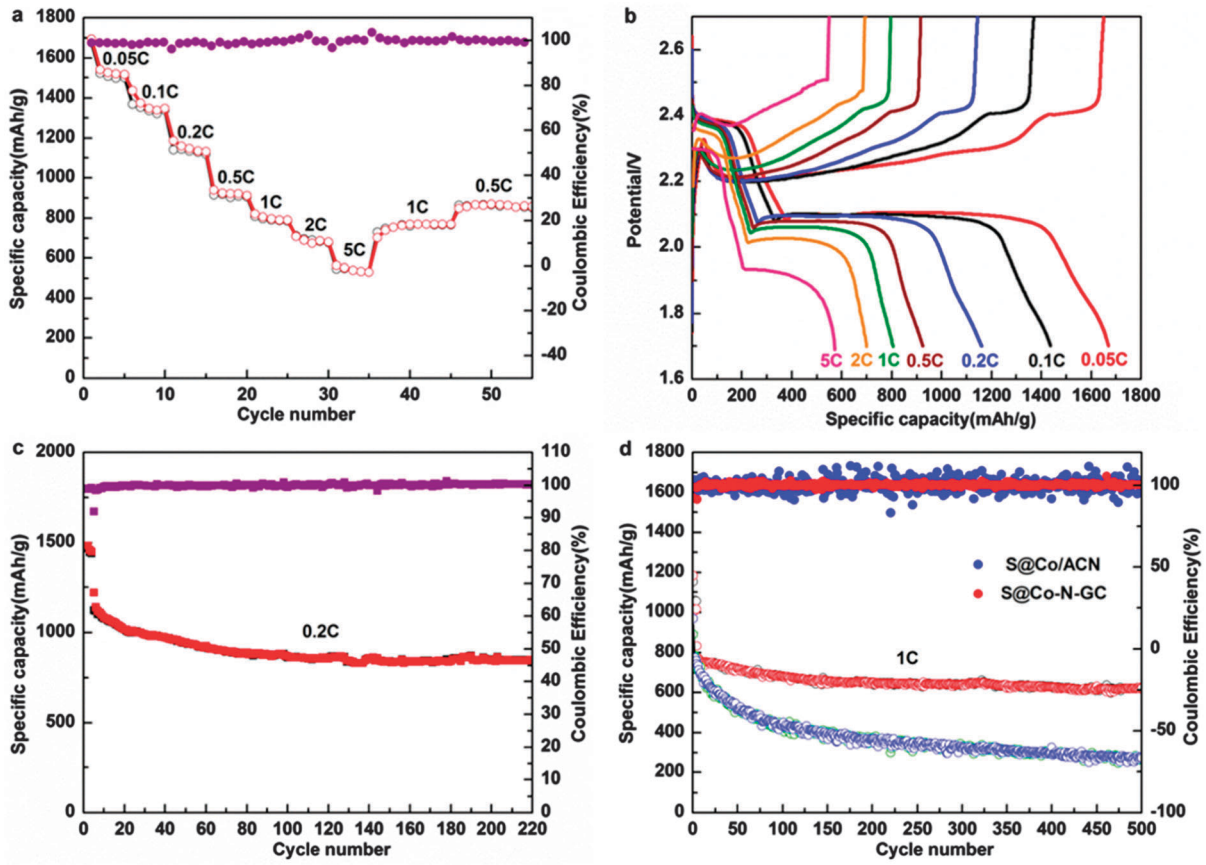

Fig. 5 (a) The rate capability of the S@Co–N-GC composite electrode at increasing current rates from 0.05C to 5C. (b) Its corresponding voltage-capacity profiles at various rates. (c) Cycling performance and coulombic efficiency of the S@Co–N-GC composite electrode at 0.2C. (d) Cycling performance and coulombic efficiency comparisons between the S@Co–N-GC and the S@Co/ACN composite electrodes at 1C.

be attributed to the firm chemical interaction between the Co-pyridinic-N enriched GC and polysulfides.

Good capacity retention over long cycles is crucial for the practical application of Li–S batteries. The cycling performance of the S@Co–N-GC composite electrode is shown in Fig. 5c and d. For comparison, *ex situ* synthesized Co/ACN composite was also employed as a sulfur host and the cycling performance of the obtained S@Co/ACN composite electrode was performed under the same conditions as that of the S@Co–N-GC composite electrode. At the current rate of 0.2C, the S@Co–N-GC composite electrode could deliver a high initial reversible capacity of 1440 mA h^{-1} g^{-1}, and this capacity decreased to 870 mA h^{-1} g^{-1} after 100 cycles, and to 850 mA h^{-1} g^{-1} after 200 cycles, with a slow capacity decay rate of 0.023% per cycle. When the current rate was increased to 1C, it could also deliver 1150 mA h^{-1} g^{-1} initially and could be maintained at 625 mA h^{-1} g^{-1} after a prolonged 500 cycles. The voltage profiles of the S@Co–N-GC composite electrode at different cycles are displayed in Fig. S4 (ESI†). It is obvious that there is no apparent voltage degeneration even after 500 cycles, indicating the excellent cycling stability. As for the S@Co/ACN composite electrode, it could only deliver an initial reversible capacity of 968 mA h^{-1} g^{-1} at the current rate of 1C, and this capacity rapidly faded to 275 mA h^{-1} g^{-1} after 500 cycles. For the S@Co–N-GC composite electrode, the efficiency was maintained at almost 100% at both 0.2C and 1C during the cycling, while the value for the S@Co/ACN electrode was rather unstable, especially at the larger current rate. These results indicate that the existence of Co was likely to help enhance the specific capacity, especially at low current rates, by effectively transforming long-chain PSs to short-chain ones. In order to further confirm the role of Co, the S/Super P and S/Co/Super P electrodes were cycled at a current rate of 0.2C. As shown in Fig. S5b (ESI†), the S/Co/Super P electrode exhibited an initial specific capacity of 1214 mA h^{-1} g^{-1} and retained a stable capacity of 450 mA h^{-1} g^{-1} after 200 cycles of charge/discharge. In comparison with pristine Super P, Co/Super P resulted in a 25% enhancement in capacity. Moreover, the S@Co/ACN electrode also exhibited excellent specific capacity over the S@ACN electrode (Fig. S6, ESI†). More notably, the S/Co/Super P electrode showed more stable coulombic efficiency upon cycling. Therefore, Co is promising as an electrocatalyst to convert long-chain polysulfides to short-chain ones and even to Li_2S efficiently during discharging, such as for the reported Ni/Pt,[31] which is conducive to the capacity increasing. Moreover, the improved cycle performance of the S@Co–N-GC composite electrode can also be attributed to the nitrogen doping on the GC surface, especially the pyridinic-N, which can provide one pair of lone electrons for trapping polysulfide species through the strong binding of Li in Li_2S_n with N atoms. This was also demonstrated by our previous work in which the adsorption energy of Li_2S_n on pyridinic-N enriched carbon surface was enhanced by about −30 kcal mol^{-1} with respect to a pristine carbon surface.[32] In this case, soluble Li_2S_n can be absorbed on the N-GC surface and can be readily further reduced and oxidized *via* surface-mediated and Co-catalytic processes, which can significantly improve the S utilization and alleviate the shuttling of polysulfides to the anode, and thus the coulombic efficiency of the S@Co–N-GC composite electrode is very close to 100%.

Furthermore, in order to identify the synergistic catalytic effect of Co–N, we examined the performance of N-GC and Co–GC composites after removing the Co metal or nitrogen under identical conditions, respectively. On one hand, the as-prepared Co–N-GC composite was immersed in HCl solution to remove mostly Co (ESI†). As shown in Fig. S7 (ESI†), the S@N-GC composite exhibited a much inferior rate capability and lower capacity and coulombic efficiency than the S@Co–N-GC composite. It only delivered an initial specific discharge capacity of 1010 mA h^{-1} g^{-1}, even at a low current rate of 0.05C. The inferior rate capability of S@N-GC can be ascribed to the absence of Co, demonstrating that metallic Co is conducive to the capacity increasing. On the other hand, the as-prepared ZIF-67 material was subjected to heating at 1000 °C for 3 h in N_2. The N-functionalities were mostly eliminated after this heating treatment,[37] and the yield material was denoted as Co–GC. As shown in Fig. S8a (ESI†), compared with the Co–N-GC material, the S@Co-GC could deliver a relatively high specific discharge capacity of 1376 mA h^{-1} g^{-1} but a reversible charge capacity of 1173 mA h^{-1} g^{-1} with a coulombic efficiency of only 85.2%. The low coulombic efficiency can be ascribed to the absence of N. The capacity faded to 1119 mA h^{-1} g^{-1} after three cycles. In addition, the cycling performance of S@Co-GC was observably reduced after removing the N composite, as shown in Fig. S8b (ESI†). It could also deliver 1065 mA h^{-1} g^{-1} initially at the current rate of 1C, but the capacity rapidly faded to 382 mA h^{-1} g^{-1} after 200 cycles. This result further confirmed that Co is conducive to the capacity increasing and that the doped-N is apt to improving cycle performance by facilitating the oxidation of $Li_2S_6 \rightarrow Li_2S_8 \rightarrow S_8$, thus improving the S utilization. These control experiments clearly suggest the important synergetic effect between metallic Co and N in determining the activity of the Co–N-GC composite for Li–S batteries. In addition, although the Co–N-GC and Co/ACN composites had similar surface areas (Fig. S9, ESI†) and absorbability of lithium polysulfides (Fig. 6), their electrochemical performances were rather different, as the above results showed, suggesting that the *ex situ* synthesized Co/ACN composite is not as effective as the *in situ* synthesized Co–N-GC in preventing lithium polysulfide shuttling. This is possibly because Co and N were mixed by just simple physical mixing in the Co/ACN composite. The results revealed that it is very crucial to rationally design an electrode in which not only an ideal matrix is utilized that could entrap the intermediate polysulfides effectively but also the synergistic catalytic effect of Co–N for S redox could be effectively improved.

In conclusion, a Co–N-GC composite with a structure inherited from MOFs was designed and synthesized by a facile method, which was very effective to entrap polysulfides physically and electrocatalytically in a Li–S battery, resulting in significantly improved electrochemical performance. The cathode with 70 wt% of S in the total electrode weight exhibited a high specific capacity and excellent rate performance up to 5C. It could deliver a high specific discharge capacity of 1670 mA h^{-1} g^{-1}, which is almost the theoretical capacity of S, and an extremely

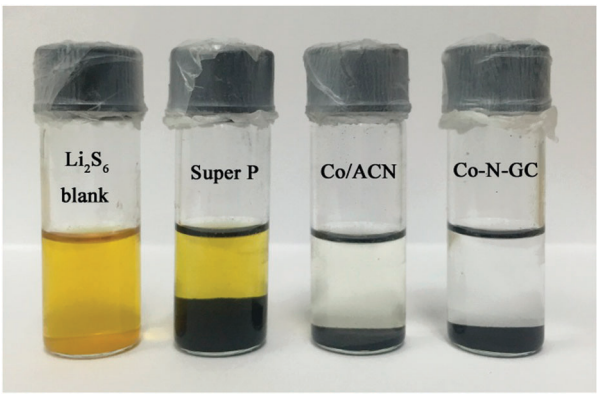

Fig. 6 Sealed vials of Li_2S_6/DME&DOXL solutions, after contact with Super P, as-prepared Co/ACN and Co–N-GC composites.

high coulombic efficiency of 98.9% at the current rate of 0.05C. The multi-functional effects were thus integrated in a S cathode. In terms of catalyzing capabilities, the Co–N-GC composite was then demonstrated to have a dual-catalyzing effect for S reduction and oxidation processes, where Co, doped-N and N-GC matrix acted according to their own role in the synergistic system. The present study thus demonstrates that the S@Co–N-GC electrode has a great potential to be used in low-cost and high-energy Li–S batteries and provides important guidance to the design of a multi-functional sulfur host for Li–S batteries.

Acknowledgements

We gratefully acknowledge the financial support from the National 973 Program (2015CB251102), the Key Project of NSFC (U1305246, 21321062), and the Fundamental Research Funds for the Central Universities (20720150042).

References

1 P. G. Bruce, S. A. Freunberger, L. J. Hardwick and J. M. Tarascon, *Nat. Mater.*, 2012, **11**, 19–29.
2 J. Wang, J. Yang, C. Wan, K. Du, J. Xie and N. Xu, *Adv. Funct. Mater.*, 2003, **13**, 487–492.
3 A. Manthiram, Y. Fu, S. H. Chung, C. Zu and Y. S. Su, *Chem. Rev.*, 2014, **114**, 11751–11787.
4 H. B. Wu, S. Wei, L. Zhang, R. Xu, H. H. Hng and X. W. Lou, *Chem. – Eur. J.*, 2013, **19**, 10804–10808.
5 X. Wang, Z. Zhang, Y. Qu, Y. Lai and J. Li, *J. Power Sources*, 2014, **256**, 361–368.
6 J. Wang, J. Chen, K. Konstantinov, L. Zhao, S. H. Ng, G. X. Wang, Z. P. Guo and H. K. Liu, *Electrochim. Acta*, 2006, **51**, 4634–4638.
7 X. Liang, Y. Liu, Z. Wen, L. Huang, X. Wang and H. Zhang, *J. Power Sources*, 2011, **196**, 6951–6955.
8 W. Zhou, Y. Yu, H. Chen, F. J. DiSalvo and H. D. Abruna, *J. Am. Chem. Soc.*, 2013, **135**, 16736–16743.
9 X. Liang, Z. Wen, Y. Liu, H. Zhang, L. Huang and J. Jin, *J. Power Sources*, 2011, **196**, 3655–3658.
10 W. Zhou, X. Xiao, M. Cai and L. Yang, *Nano Lett.*, 2014, **14**, 5250–5256.
11 M. Oschatz, S. Thieme, L. Borchardt, M. R. Lohe, T. Biemelt, J. Bruckner, H. Althues and S. Kaskel, *Chem. Commun.*, 2013, **49**, 5832–5834.
12 C. Liang, N. J. Dudney and J. Y. Howe, *Chem. Mater.*, 2009, **21**, 4724–4730.
13 X. Ji, K. T. Lee and L. F. Nazar, *Nat. Mater.*, 2009, **8**, 500–506.
14 Z. Wang, B. Wang, Y. Yang, Y. Cui, Z. Wang, B. Chen and G. Qian, *ACS Appl. Mater. Interfaces*, 2015, **7**, 20999–21004.
15 Z. Wang, Z. Dou, Y. Cui, Y. Yang, Z. Wang and G. Qian, *Microporous Mesoporous Mater.*, 2014, **185**, 92–96.
16 S. Evers and L. F. Nazar, *Chem. Commun.*, 2012, **48**, 1233–1235.
17 A. J. Amali, J.-K. Sun and Q. Xu, *Chem. Commun.*, 2014, **50**, 1519–1522.
18 H. Yue, Z. Shi, Q. Wang, Z. Cao, H. Dong, Y. Qiao, Y. Yin and S. Yang, *ACS Appl. Mater. Interfaces*, 2014, **6**, 17067–17074.
19 W. Xia, A. Mahmood, R. Zou and Q. Xu, *Energy Environ. Sci.*, 2015, **8**, 1837–1866.
20 W. Xia, J. Zhu, W. Guo, L. An, D. Xia and R. Zou, *J. Mater. Chem. A*, 2014, **2**, 11606.
21 H. Furukawa, K. E. Cordova, M. O'Keeffe and O. M. Yaghi, *Science*, 2013, **341**, 1230444.
22 M. Eddaoudi, J. Kim, N. Rosi, D. Vodak, J. Wachter, M. O'Keeffe and O. M. Yaghi, *Science*, 2002, **295**, 469–472.
23 B. Liu, H. Shioyama, T. Akita and Q. Xu, *J. Am. Chem. Soc.*, 2008, **130**, 5390–5391.
24 R. Banerjee, A. Phan, B. Wang, C. Knobler, H. Furukawa, M. O'Keeffe and O. M. Yaghi, *Science*, 2008, **319**, 939–943.
25 L. Zhang, H. B. Wu, S. Madhavi, H. H. Hng and X. W. Lou, *J. Am. Chem. Soc.*, 2012, **134**, 17388–17391.
26 Q. Pang, D. Kundu, M. Cuisinier and L. F. Nazar, *Nat. Commun.*, 2014, **5**, 4759.
27 H. Yao, G. Zheng, P.-C. Hsu, D. Kong, J. J. Cha, W. Li, Z. W. Seh, M. T. McDowell, K. Yan and Z. Liang, *Nat. Commun.*, 2014, **5**, 3943.
28 X. Liang, C. Hart, Q. Pang, A. Garsuch, T. Weiss and L. F. Nazar, *Nat. Commun.*, 2015, **6**, 5682.
29 J. Zheng, J. Tian, D. Wu, M. Gu, W. Xu, C. Wang, F. Gao, M. H. Engelhard, J.-G. Zhang and J. Liu, *Nano Lett.*, 2014, **14**, 2345–2352.
30 G. Babu, K. Ababtain, K. Y. Ng and L. M. Arava, *Sci. Rep.*, 2015, **5**, 8763.
31 H. Al Salem, G. Babu, C. V. Rao and L. M. Arava, *J. Am. Chem. Soc.*, 2015, **137**, 11542–11545.
32 J.-J. Chen, R.-M. Yuan, J.-M. Feng, Q. Zhang, J.-X. Huang, G. Fu, M.-S. Zheng, B. Ren and Q.-F. Dong, *Chem. Mater.*, 2015, **27**, 2048–2055.
33 J. Pels, F. Kapteijn, J. Moulijn, Q. Zhu and K. Thomas, *Carbon*, 1995, **33**, 1641–1653.
34 X. Wang, J. Zhou, H. Fu, W. Li, X. Fan, G. Xin, J. Zheng and X. Li, *J. Mater. Chem. A*, 2014, **2**, 14064–14070.
35 Z. Xiang, Y. Xue, D. Cao, L. Huang, J. F. Chen and L. Dai, *Angew. Chem., Int. Ed.*, 2014, **53**, 2433–2437.
36 S. S. Zhang, *J. Power Sources*, 2013, **231**, 153–162.
37 Z. Li, Z. Xu, H. Wang, J. Ding, B. Zahiri, C. M. Holt, X. Tan and D. Mitlin, *Energy Environ. Sci.*, 2014, **7**, 1708–1718.

